Microbubble Generation for Removal of Inclusions from Liquid Melts and Their Measurement and Size Distribution Using the LiMCA System

Rohit Tiwari, Mihiela M. Isac, and Roderick I. L. Guthrie

Abstract

Non-metallic inclusions less than 50μm are presently impossible to be removed during typical liquid metal processing operations, even though their presence can have a negative impact on the properties of final products. The major purposes of injecting gas and generating microbubbles within a liquid metal bath include superior intermixing of reactants, enhancement of mass transfer or chemical reaction rates, as well as facilitating the removal of deleterious inclusions. Previous studies have shown that ~500μm bubbles are required to float out sub-50μm diameter particles/inclusions in tundish-type scenarios. Our current work demonstrates that microbubbles having a size range of around 500μm can be generated in a novel experimental apparatus using high-speed rotational shear at very low gas flow rates. Additionally, a new LiMCA (liquid metal cleanliness analyzer) setup was used to measure the sizes of microbubbles generated in low melting point alloys, for different rotational speeds and injected gas flow rates. The successful detection and measurement of bubbles using the new setup proved that the theory behind LiMCA can be used for microbubble/inclusion monitoring in various liquid melts.

Keywords

Inclusion · Microbubble · Steel refining · Liquid Metal Cleanliness Analyzer (LiMCA)

1 Introduction

Over the years, the demand for cleaner steel continues to increase. The cleanliness of steel depends on the amount, morphology, density, and size distribution of non-metallic inclusions in steel. It is well known that the presence of inclusions in metals can cause detrimental effects on mechanical properties. A clean steel entails minimizing large inclusions ~100μm, whilst avoiding inclusions larger than the critical size that are harmful for a given steel product. Inclusion removal by bubble floatation/gas dispersion has been widely accepted as a practical approach for improving metal cleanliness in molten steel. The process injects a non-reactive gas (argon) into the liquid steel, and then floating out non-wetted inclusions to the top surface by their attachment to the surfaces of rising gas bubbles. Unfortunately, this static bubbling technique does not remove inclusions below ~50μm within liquid steel flowing through a tundish' since the bubbles formed are too large (ellipsoidal and spherical cap), are too fast, and are too few. Conversely, these larger bubbles float rapidly upwards (because of their higher buoyancy forces and shorter residence time compared to the smaller ones), to entrain any overlying phase of mould powder/slag above the steel. Meantime, the smaller inclusions have little buoyancy and follow the liquid flow. Computational fluid dynamics modelling [1] had shown that 500μm bubbles would be needed to float out the <50μm alumina particles. This was arrived at during some previous research at the MMPC (McGill Metals Processing Centre), when the injection of air into the full-scale

R. Tiwari · M. M. Isac (✉) · R. I. L. Guthrie
McGill Metals Processing Centre, McGill University, Montreal, Canada
e-mail: mihaiela.isac@mcgill.ca

Proceedings of the 62nd Conference of Metallurgists, COM 2023, https://doi.org/10.1007/978-3-031-38141-6_34

delta-shaped water model of a commercial ladle and tundish set-up located in the water modelling laboratory, led to the production of 4–6 mm size bubbles. These bubbles separated from the water down flow to create an upwelling bubble plume of water surrounding the ladle shroud, resulting in the formation of a "Slag/Steel Open Eye," or SOE.

The recent work at the MMPC [2] has shown that it is possible to generate microbubbles in the range of ~500μm in both water and low melting alloy using a novel piece of equipment (called as microbubble generator). This technique uses high-speed rotational shearing at very low gas flow rates. The present work addresses the measurement of the microbubbles using a new LiMCA (Liquid Metal Cleanliness Analyzer) set-up, for different rotational speeds and injected gas flow rates. The successful detection and measurement of bubbles using the new set-up proved that the theory behind LiMCA can be used for microbubble/inclusion monitoring in various liquid melts.

1.1 Technical Development of LiMCA

The LiMCA works on the Electric Sensing Zone (ESZ) principle first considered by J.C. Maxwell and first exploited by Wallace Coulter back in 1953, for aqueous systems. Its direct extension to the metallurgical industry was first proposed and exploited by Guthrie and Doutre in late 1979 with the first working instrument designed to detect inclusions in liquid aluminum processing operations [3]. The years from 1980 to 2000 saw a remarkable development of LiMCA as several variants of it were designed for a variety of metal systems such as aluminum, magnesium, copper, iron, and steel, etc. As a result, commercial production models are now being marketed by ABB and Alcan (LiMCA CM® for Aluminum) and Heraeus Electo-Nite (ESZpas for steel). While previous researchers have shown that the LiMCA system can detect solid inclusion in liquid metals, the same principle can be used to detect and measure the microbubbles within a liquid bath. Recent activities in its continuing development at the MMPC are aimed at improving LiMCA equipment for physical modeling experiments and detecting microbubbles in water, or low-melting liquid metals.

2 Experimental Set-Up of LiMCA Sensor

2.1 Working Principle

The LiMCA sensor is primarily based on the ESZ principle. A schematic of the ESZ method for measuring the size of non-conducting inclusions/gas bubbles is shown in Fig. 1. The fluid containing a suspension of the inclusion particles/gas bubble is drown in to pass through the narrow orifice. Two electrodes are used so as to apply a constant electrical current supply (I) through the orifice. When no particles/bubbles pass with the fluid through the orifice, the resistance (R) across the electrodes is due only to the conductive fluid. This produces a potential difference V = (IR) across the electrodes, which is recorded as the baseline output. If a particle/bubble enters the orifice, thereby displacing its own volume of fluid as voltage pulse/peak is recorded. Since the conductive fluid in the orifice is now replaced by a comparatively less conductive particle/bubble, the resistance across the orifice changes to (R + ΔR), and the potential difference across the electrodes jumps to I (R + ΔR). This jump in voltage as the particle/bubble passes through the orifice is recorded, and its magnitude is an indication of the size of the particle/bubble [5–7].

2.2 Fundamentals of LiMCA Operation

During the physical experiment with the LiMCA sensor, the number of peaks detected is equal to the number of particles/bubbles sampled, and the height of the peaks is related to the particle/bubble sizes according to Eq. 1 [7].

$$\Delta V = \frac{4\rho_e I d^3}{\pi D^4} = k d^3 \tag{1}$$

In Eq. 1, ΔV is the change in voltage when the particle/bubble passes through the orifice, ρ_e is the electrical resistivity of the working fluid, I is the constant current flowing through the orifice, d is the diameter of the particle/bubble, and D is the diameter of the orifice. For a given LiMCA sensor set-up (constant current supply and orifice diameter), the term $\frac{4\rho_e I}{\pi D^4}$ will be

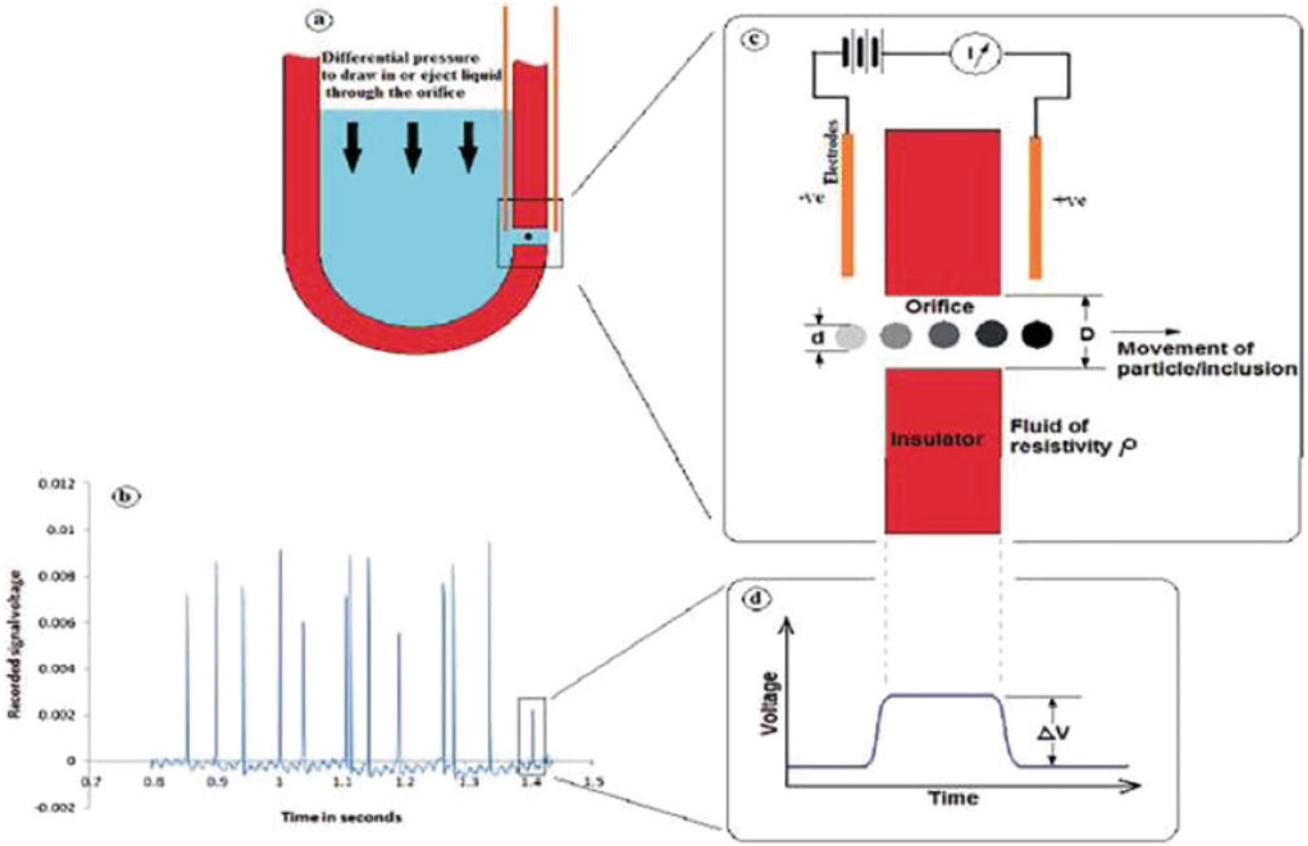

Fig. 1 Electric Sensing Zone (ESZ) principle for inclusion detection systems [4]

constant irrespective of particle/bubble size and can be termed as constant k as shown in Eq. 1. This equation was derived from Maxwell's approximations, which shows that the particles are so dispersed in the medium that they do not in any way alter the electric field within the orifice, except at positions near the particle surface. The individual voltage peaks in the signal are, however, far too small in magnitude to be accurately measured by a data acquisition system, so the raw signals from the detector must be amplified linearly by a factor α.

$$\Delta V_{\text{amplified}} = \alpha k d^3 = k' d^3 \tag{2}$$

For the present sensor setup, the amplifying factor was chosen as 1000, considering a total output signal swing of 0–5 V for the present the data acquisition system used in analysis.

2.3 Set-Up of the Microbubble Generator and LIMCA System

The experimental set-up of the LiMCA sensor used for microbubble detection is shown in Fig. 2 (left). It consists of a borosilicate glass tube containing a small orifice called the "Electric Sensing Zone" located near the bottom of the closed-end tube. Two electrodes are used to apply the necessary constant electrical current (I) supplied from a Direct Current (DC) heavy-duty lead-acid car battery of 12 V, as the power supply system. The glass tube and the electrodes are submerged into a cylindrical container filled with the experimental fluid; water or liquid metal. The output signal from the sensor (potential difference between the electrodes) is transmitted to the data acquisition system via an amplifier (as discussed in the previous section). The microbubbles are generated via a microbubble generator device fastened to the vessel. The microbubble generator is connected to a mixer device that creates a controlled, high-speed, rotational shear in the fluid, as shown in Fig. 2 (right). Also, a flowmeter is connected to the microbubble generator, allowing adjustments to the gas flow rate. Thus,

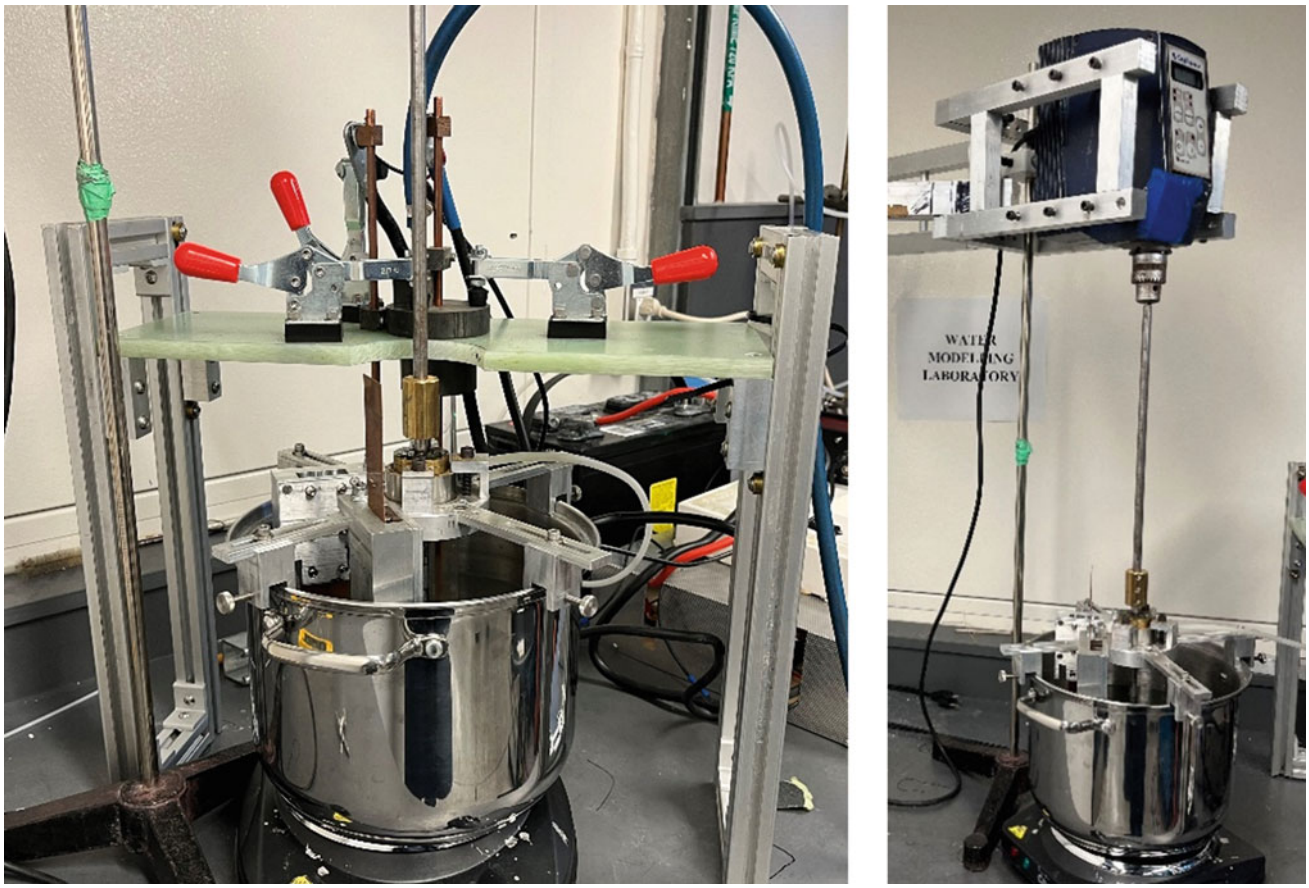

Fig. 2 Experimental set-up for microbubble measurement including LiMCAsystem (left) and the mixer device, connected to the microbubble generator (right)

microbubbles of various size ranges can be generated depending on the rotational speeds of the microbubble generator and gas injection rate. Detailed design and functioning of the microbubble generator can be found in our previous work [2]. The top of the LiMCA tube is connected to the vacuum unit through a hollow pipe allowing suction of the fluid into the tube through the orifice as per requirement.

2.4 Signal Processing and Data Acquisition

Raw data obtained as the output signal from the LiMCA sensor, following subsequent amplification, would merely consist of a number of transient voltage pulses corresponding to each particle being counted. Since the bubble generally takes less than a millisecond to pass through the orifice, these voltage pulses were very narrow. Proper signal acquisition and analysis were essential to obtain useful information from electronic signals. The amplified signal was fed to an instruNet controller, a data acquisition device enabling data flow from the equipment to be transferred to a computer, via the DASYLab software (Fig. 3). In the DASYLab software, the voltage signals were classified into several appropriately chosen bins. Counters were used to store the number of bubbles falling into each size range or bin. Finally, the percentage of bubbles in each bin is obtained by dividing the value of its corresponding counter by the total bubble count and displayed as a histogram. For the present study, the microbubbles were classified into nine different size ranges, or bins uniformly distributed between 0.03 V and 0.12 V.

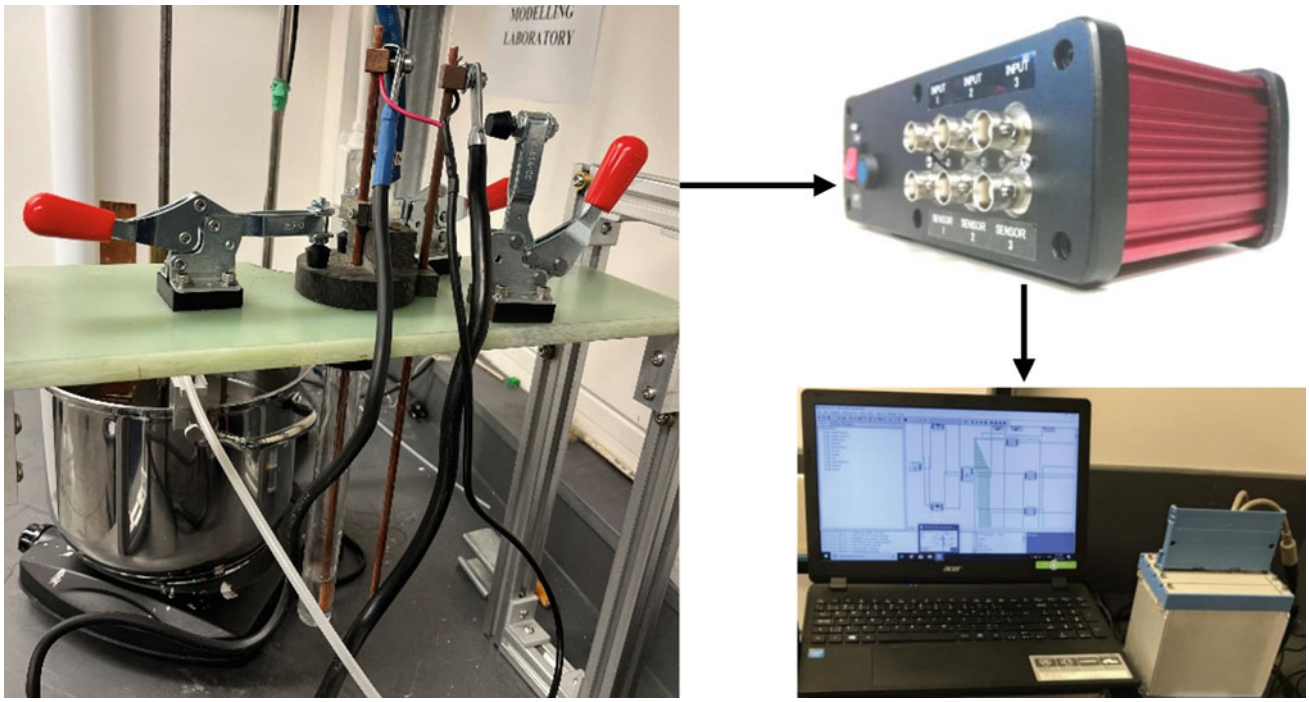

Fig. 3 Data acquisition system to transfer signal from LiMCA sensor (left) to amplifier (right-top) and then to the DASYLab via instruNet controller (right-bottom), and then to the computer

3 Results and Discussion

3.1 LiMCA Sensor Calibration

It should be noted that while the algorithm itself should classify a bubble based on its diameter, it is the signal voltage that it is measuring. A calibration test was needed to convert voltage bins into the appropriate bubble size ranges. For this, six different wires with known diameters were passed through the orifice, and their corresponding voltage peak was noted; a total number of 42 tests were done. Here one important point is that the equation of peak voltage signal for a cylindrically shaped wire while passing through the probe will be modified as follows:

$$\Delta V = \frac{4\rho_e I d^2}{\pi D^4} = \alpha k d^2 = k' d^2 \tag{3}$$

As discussed before, for a specific setup (constant current and orifice diameter), the value of k' in Eq. 3 will be the same irrespective of bubble size passing through the probe. The objective of the calibration test of the LiMCA probe was to find out this constant value. A regression analysis was performed based on the experimental values to get a k' value equal to 0.166. This regression model's overall adjusted R square value was found to be 0.91, indicating good predictability with experimental results. Fig. 4 compares the experimental voltage peak signal observed with the voltage value calculated using the predicted k' value.

Based on the predicted value of the constant k' during the calibration test, bubble sizes were calculated for each bin using Eq. 2. Table 1 shows the voltage range and corresponding bubble size for each bin number.

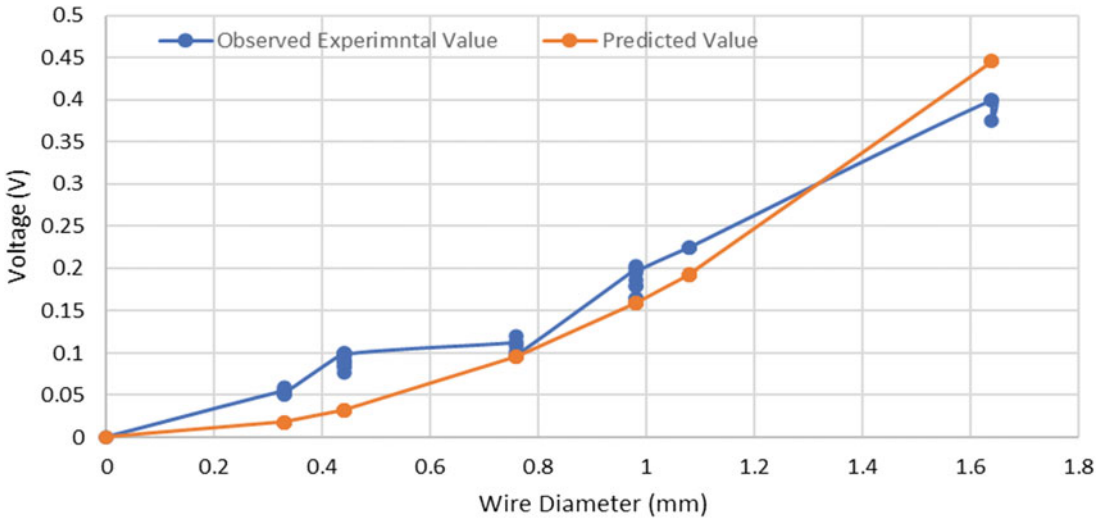

Fig. 4 Comparison of experimental voltage signal with the predicted value

Table 1 Voltage and bubble size range for each bin number

Bin number	Voltage range (V)	Bubble size range (mm)
1	0.03–0.04	0.57–0.62
2	0.04–0.05	0.62–0.67
3	0.05–0.06	0.67–0.71
4	0.06–0.07	0.71–0.75
5	0.07–0.08	0.75–0.78
6	0.08–0.09	0.78–0.82
7	0.09–0.1	0.82–0.84
8	0.1–0.11	0.84–0.87
9	0.11–0.12	0.87–0.9

3.2 Visual Observation

Figure 5 shows the typical voltage pulses observed during the passage of microbubbles, generated via a microbubble generator with an airflow rate of 100 mL/min for four different rotational speeds of 550, 650, 750, and 950 rpm. A higher number of voltage peak signals was observed with an increase in rotational speed. This suggests that more bubbles are formed with an increase in rotational speed. At higher rotational speeds, turbulence shearing force within a liquid bath, lead to a greater degree of bubble breakage and fragmentation.

3.3 Effect of Gas Injection Rate

Figure 6 shows the percentage of bubbles falling in different bins or size ranges, for different air flow rates, at a rotational speed of 850 RPM. As shown in Fig. 6, with an increase in gas flow rate, the bubble frequency decreases for lower bin number (bin 1–3). Similarly, the bubble frequency increases with an increase in flow rates for higher bin number (bin 6–9). As shown in Table 1, bin 1–3 represents the bubble size range between 0.57 mm and 0.71 mm and bin 6–9 represents the bubble size range between 0.78 mm and 0.9 mm. This implies that at lower gas flow rate, more number of bubbles formed are in the smaller size range (0.57–0.71 mm). Similarly, at higher flow rate, percentage of bigger sized bubble (0.78–0.9 mm) is higher. This trend suggests that with an increase in flow rate, bubble size increases, agreeing with the theoretical understanding of bubble formation with the increase in flow rate [2, 8, 9].

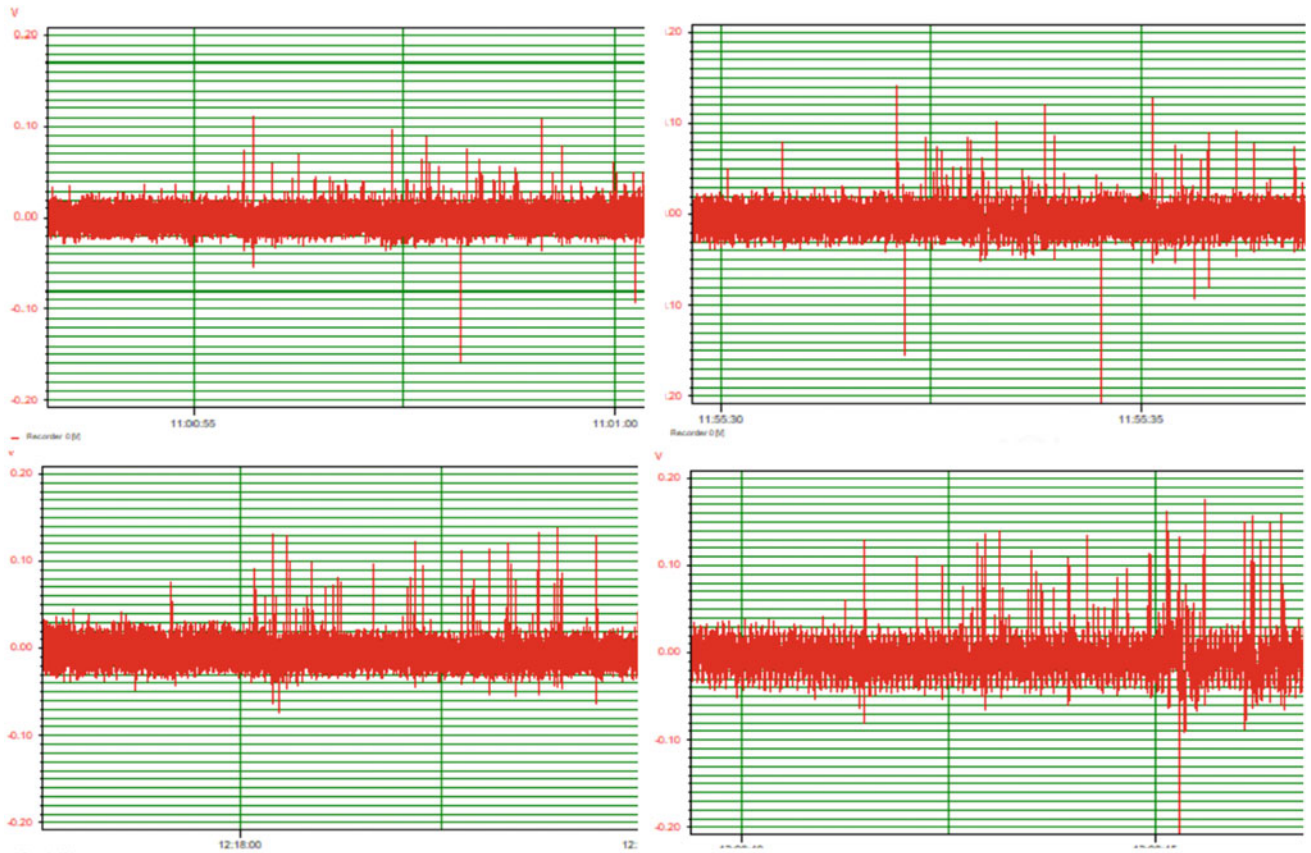

Fig. 5 Typical voltage pulses observed during the passage of microbubbles, generated at an airflow rate of 100 mL.min^{-1} and four different rotational speeds of 550 RPM (top-left), 650 RPM (top right), 750 RPM (bottom-left), and 950 RPM (bottom-right)

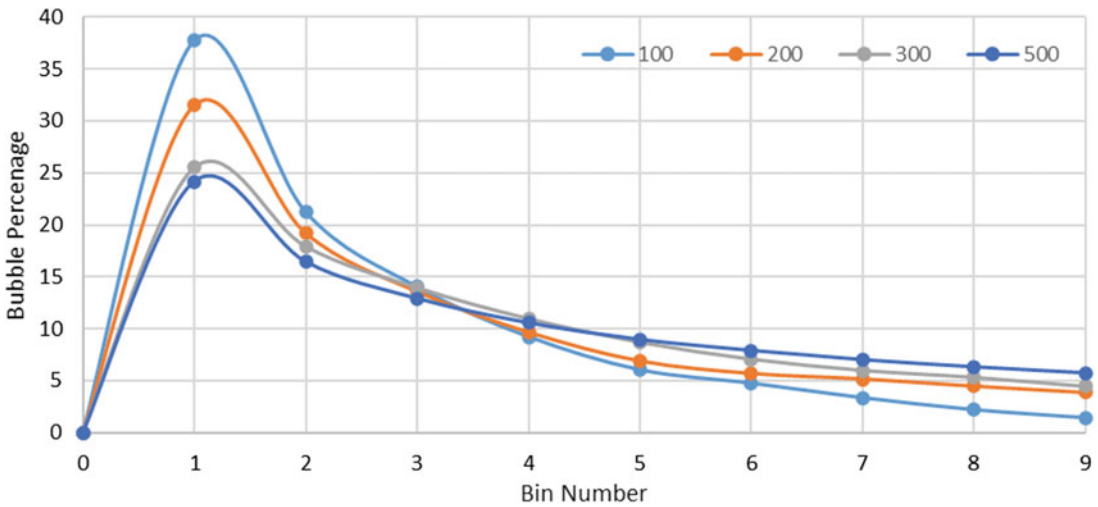

Fig. 6 Bubble percentage in various bin for different air flowrates (mL/min) at a rotational speed of 850 RPM

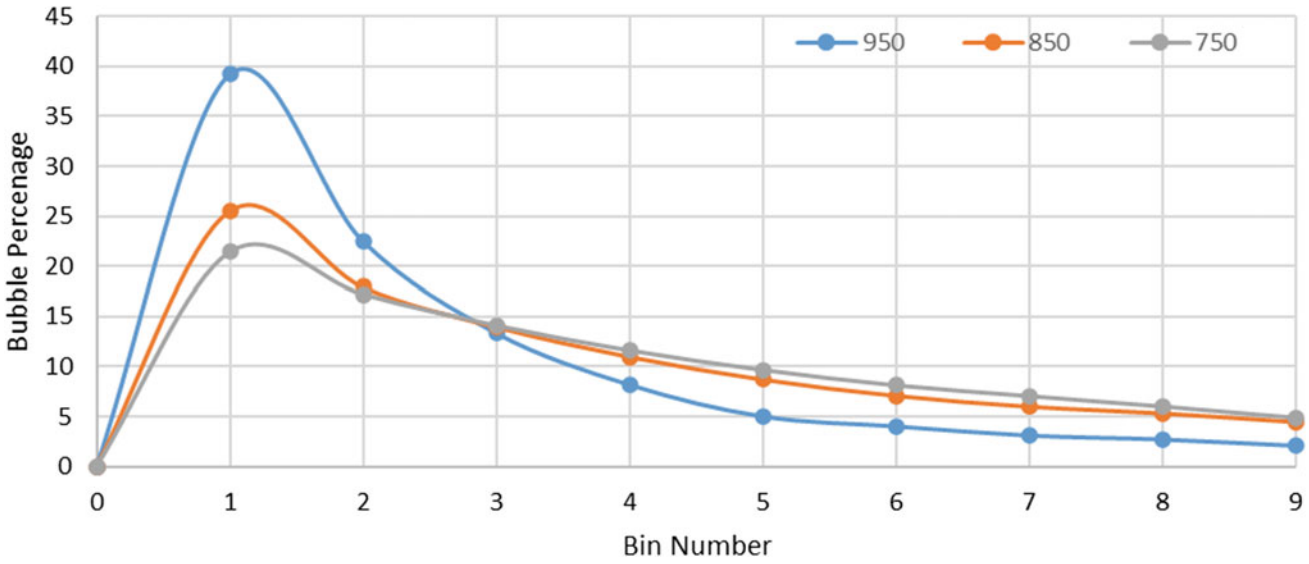

Fig. 7 Bubble percentage falling in various bin for different rotational speeds at an air flowrates of 300 mL/min

3.4 Effect of Rotational Speed

Figure 7 shows the bubble percentage falling in different bins or size ranges for different rotational speeds of the microbubble generator at an air injection rate of 300 mL/min. As shown in Fig. 7, with an increase in rotational speed, the bubble frequency increases for lower bin number (bin 1–3). Similarly, the bubble frequency decreases with an increase in rotational speed for higher bin number (bin 5–9). As shown in Table 1, bin 1–3 represents the bubble size range between 0.57 mm and 0.71 mm and bin 5–9 represents the bubble size range between 0.75 mm and 0.9 mm. This implies that at higher rotational speed, more number of bubbles formed are in the smaller size range (0.57–0.71 mm). Similarly, at lower rotational speed, percentage of bigger sized bubble (0.75–0.9 mm) is higher. This trend suggests that with an increase in rotational speed, bubble size decreases, in agreement with our theoretical understanding of bubble formation with increase in flow rate [2, 9].

4 Conclusions

The following conclusions can be drawn from the current investigation:

1. A new and improved LiMCA sensor has been developed which can be used to detect and measure the sizes of microbubbles.
2. The trend of bubble size versus RPM and air flow rate observed with experimental measurement through LiMCA sensor was similar to those observed in previous work [2].
3. Successful detection and measurement of bubble size using LiMCA sensor shows that the theory behind LiMCA supports the monitoring of microbubble/inclusion, in various liquid melts.

Acknowledgments The authors thank the Natural Sciences and Engineering Research Council of Canada (NSERC), the Quebec Centre of Aluminum Research and Development (CQRDA), as well as member companies of the McGill Metals Processing Centre (MMPC) for their financial support.

References

1. Chattopadhyay K, Isac M, Guthrie RIL (2011) The concept of micro-bubbles within a tundish – physical and mathematical modelling. Metec Insteelcon, Dusseldorf, pp 1–9

2. Panicker A, Lu D, Tiwari R, Calzado L, Isac MM, Guthrie RIL (2022) A novel experimental set-up for generating microbubbles, for removal of inclusions. In: Proceedings of the 61st conference of metallurgists COM (2022). Montreal, pp 369–381
3. Doutre DA, Guthrie RIL (1983) Method and apparatus for the detection and measurement of particulates in molten metal. US patent, 4555662
4. Isac M, Chakraborty A, Calzado L, Guthrie R (2011) Development of an Aqueous Particle Sensor (APSIII) System as a Research Tool for Studying the Behavior of Inclusions in Water Models of Tundish Operations. In Sensors, Sampling, and Simulation for Process Control (eds B.G. Thomas, J.A. Yurko and L. Zhang). https://doi.org/10.1002/9781118061800.ch3
5. Guthrie RIL, Li M (2001) In situ detection of inclusions in liquid metals: part I. mathematical modeling of the behavior of particles traversing the electric sensing zone. Metall Mater Trans A 32B:1067–1079
6. Li M, Guthrie RIL (2000) Numerical studies of the motion of particles in current-carrying liquid metals flowing in a circular pipe. Metall Mater Trans A 31B:357–364
7. Guthrie RIL, Li M (2001) In situ detection of inclusions in liquid metals: part II. Metallurgical applications of LiMCA systems. Metall Mater Trans A 32B:1081–1093
8. Marshall S, Chudacek MW, Bagster DF (1993) A model for bubble formation from an orifice with liquid cross-flow. Chem Eng Sci 48(11): 2049–2059
9. Ren X (2015) Bubbles generation under turbulent conditions at the steel making ladle shroud. A water modeling and CFD study McGill University, Montreal